Available Online: 17 December 2025 DOI: 10.54254/2977-3903/2025.30706

Design of a follow-me cart based on STM32

Yuan Wang[1], Dongchuan Yan[2]*

[1]Geely University, Chengdu, China
[2]Guangdong Lanrui Technology Group Co., Ltd., Foshan, China

*Corresponding Author. Email: 379564650@qq.com

Abstract. To address the various limitations inherent in traditional follow-me technologies, this study proposes an intelligent follow-me cart built on an STM32 microcontroller and Ultra-Wideband (UWB) positioning. A simplified one-dimensional positioning model is constructed using two base stations and one tag, and real-time distances between the tag and each base station are obtained through a Two-Way Ranging (TWR) algorithm. By combining these distance measurements with appropriate mathematical methods, distance-based control is implemented to enable stable tracking of a moving target. The design adopts a modular architecture that integrates the STM32 controller, motor driver, and positioning unit, together with a one-dimensional positioning model and a sliding-average filtering algorithm, effectively suppressing multipath interference and measurement noise. Experimental results show that the proposed follow-me cart achieves reliable tracking performance in low-speed scenarios.

Keywords: intelligent follow-me cart, ultra-wideband, STM32, TWR algorithm, proportional control

1. Introduction

With the rapid rise of emerging technologies such as artificial intelligence and the Internet of Things, the demand for autonomous follow-me mobile devices has increased significantly across fields including logistics distribution, service robotics, and smart warehousing. In e-commerce logistics, for instance, follow-me carts can replace manual handling and greatly improve sorting efficiency; in healthcare settings, intelligent carts that transport medicines or instruments can reduce the risk of cross-infection. However, traditional follow-me technologies suffer from several shortcomings—such as low accuracy and high susceptibility to environmental interference—which hinder broader application and development [1].

This design integrates STM32 with wireless positioning technology to develop a low-cost, high-precision intelligent follow-me cart. It is intended for use in industrial automation and public service scenarios, contributing to the advancement of intelligent control.

2. Follow-me scheme

In recent years, as intelligent driving technologies have increasingly converged with robotics, research and application of follow-me carts have made significant progress both domestically and internationally. Their core objective lies in achieving autonomous tracking of dynamic targets and coordinated operation. Current technical approaches are generally divided into two categories: vision- or LiDAR-based environmental perception solutions, and wireless ranging solutions based on positioning signals. After a comprehensive comparison of various wireless positioning technologies, this design adopts UWB as the wireless positioning method.

2.1. Structural design of the cart

The structural design of the cart must adhere to the principles of low cost, easy assembly, and strong adaptability. In this design, four DC motors are used to independently drive each wheel, providing the power output. Differential steering is employed for directional control.

2.2. Positioning scheme

In the entire control system, acquiring the target's position is fundamental to achieving autonomous following, as the positioning accuracy directly determines the precision and stability of system responses.

This design adopts a UWB-based positioning method and constructs a simplified model consisting of two base stations and one tag. The two base stations are mounted on the front frame of the cart along the horizontal direction, with a fixed separation distance *b*. The tag is placed on the object to be followed, as illustrated in Figure 1. During system operation, Base Station 0 and Base Station 1 repeatedly measure the distance to the tag, obtaining distance values *a* and *c* respectively. Based on these values, the cosine of the angle θ between the line from Base Station 0 to the tag and the baseline between Base Stations 1 and 0 is computed using the law of cosines, as shown in Equation (1). The angle θ is then obtained through inverse trigonometric functions and provided to the STM32 controller for subsequent path planning and motion control.

$$cos\theta = \frac{b^2+c^2-a^2}{2bc} \tag{1}$$

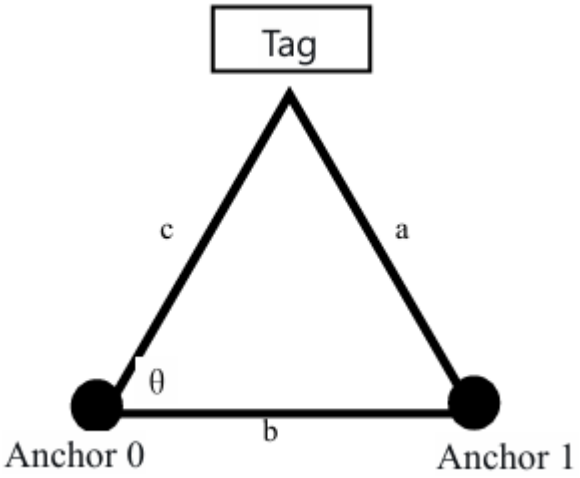

Figure 1. Positioning schematic diagram

3. Hardware design

3.1. UWB positioning module

The UWB positioning module selected for this design is the BP-TWR-30, which uses the DW1000 RF chip developed by DecaWave in the Netherlands as its core component. In terms of ranging and positioning accuracy, the module achieves a ranging error within 5 cm and supports a maximum communication distance of up to 30 m. With an added power amplifier, the effective range can be extended to over 200 m, fully meeting the system's requirements for real-time performance and high accuracy.

Base Station 0 is placed at the coordinate (0, 0), and Base Station 1 at (40, 0) (units: cm). The tag is mounted at the center of the target object. To reduce multipath interference, the antennas of the base stations and the tag must be installed at the same height as the tag and kept vertically aligned with the ground. Figure 2 shows the actual UWB modules, where (a) is Base Station 0, (b) the tag, and (c) Base Station 1.

(a) Base Station 0 (b) Tag (c) Base Station 1

Figure 2. UWB modules

3.2. Motion execution module

The cart uses 130 miniature DC geared motors, with the TB6612FNG serving as the motor driver module. To improve power management, the system power supply and motor power supply are separated to avoid mutual interference and enhance overall stability. The control modes can be switched according to the cart's operating conditions, ensuring stable motion and responsive performance across different working scenarios.

4. Implementation of the UWB positioning algorithm

4.1. TWR positioning algorithm

The Two-Way Ranging (TWR) positioning algorithm determines the distance between a tag and a base station by calculating the signal's round-trip Time of Flight (TOF), and then derives the tag's position through trilateration. This method requires both the tag and the base station to possess the capability to transmit and receive signals. During ranging, each side records timestamps of transmitted and received messages, and the time intervals are used to compute the distance between them. TWR can be categorized into Single-Sided Two-Way Ranging (SS-TWR) and Double-Sided Two-Way Ranging (DS-TWR).

Based on communication patterns, SS-TWR completes the measurement with a single bidirectional exchange, whereas DS-TWR performs two full signal exchanges, effectively eliminating clock offset errors and improving ranging accuracy, though at the cost of increased protocol complexity and implementation difficulty. Therefore, this design adopts the SS-TWR method [2, 3], as shown in Figure 3. In practical positioning systems, at least three base stations are usually deployed to form geometric constraints for trilateration. However, this design employs a simplified approach using only two base stations.

4.1.1. Single-sided two-way ranging

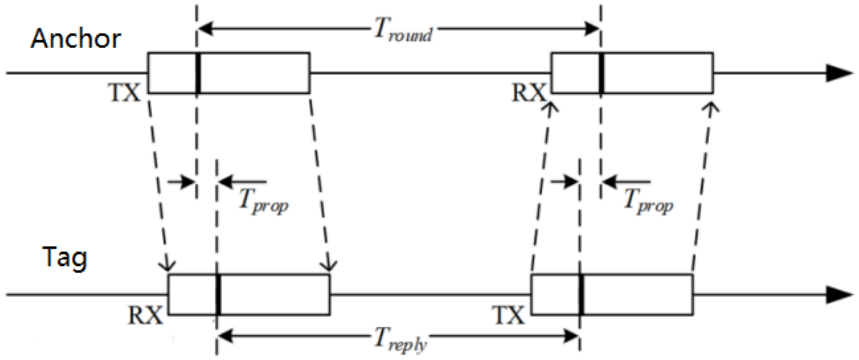

Figure 3. Single-Sided Two-Way Ranging (SS-TWR)

The SS-TWR workflow proceeds as follows: The base station first sends a message to the tag and records the transmission timestamp. After receiving this message, the tag records its reception timestamp, waits for a fixed delay Treply, then sends a reply message back to the base station and records the transmission timestamp. Upon receiving the reply, the base station records the reception timestamp [4]. By using the timestamps recorded at both ends, the time intervals of the two exchanges are computed, and the average TOF is obtained. The calculations are as follows:

$$TOF = \frac{T_{round} \times T_{reply} - T'_{round} \times T'_{reply}}{T_{round} \times T_{reply} + T'_{round} \times T'_{reply}} \tag{2}$$

where T_{round} and T_{reply} are the round-trip and reply times during the first ranging process, and T'_{round} and T'_{reply} are the corresponding values from the second measurement. The distance d is computed using the speed of light $c = 3 \times 10^8$ m/s:

$$d = TOF \times c \tag{3}$$

4.1.2. One-dimensional positioning

A coordinate system is established as shown in Figure 4. Two base stations, *A* (Base Station 0) and *B* (Base Station 1), as well as tag *C*, are deployed as illustrated. The two base stations measure their respective distances to the tag, obtaining values *a* and *c*.

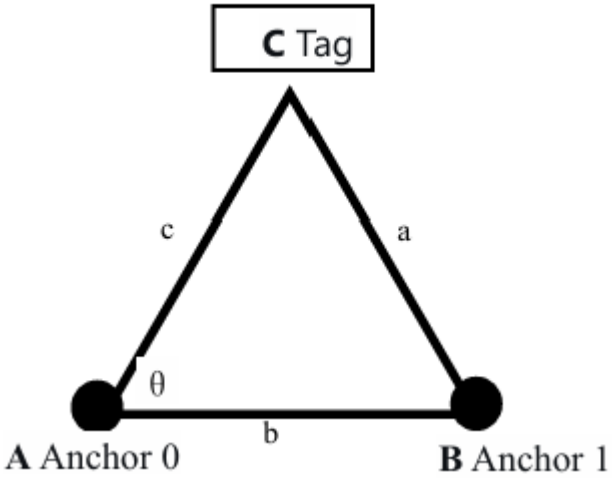

Figure 4. Positioning coordinate system

Using Equation (1), the cosine of the angle θ between Base Station 0–Tag *C* and the baseline between the two base stations is calculated. The angle θ is then obtained through an inverse trigonometric function.

Once θ is known, the relative position of the tag with respect to the cart can be determined. For example, when the distances among Base Station 0, Base Station 1, and the tag are equal, $\theta \approx 63°$. When the tag is located on the left side of the cart, θ increases (Figure 5). When the tag is located on the right side, θ decreases (Figure 6). With this relationship, the cart's movement can be controlled using θ together with the distance between any base station and the tag. For instance, if the desired following distance is set to 0.5 m, the control logic may be defined as: turn left when $\theta > 110°$; turn right when $\theta < 45°$ [5].

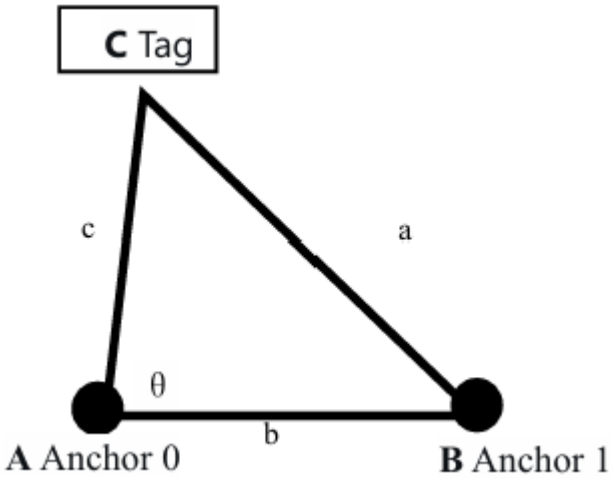

Figure 5. Tag on the left

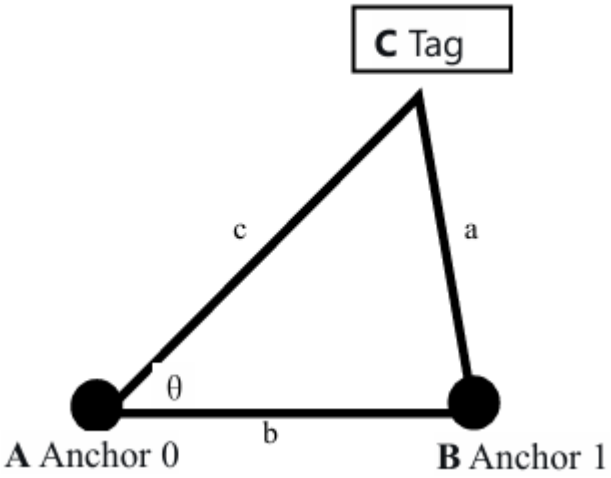

Figure 6. Tag on the right

4.1.3. Optimization of positioning accuracy

In practical ranging scenarios, measured distances may deviate due to various sources of interference. To improve measurement accuracy, this design applies a sliding average filter to suppress random noise while preserving the overall trend of valid data.

By selecting an appropriate window size, high-frequency random noise can be effectively smoothed. A larger window yields better smoothing but introduces greater latency; at the same time, the window size must exceed the noise period. Here, a window size of 5 is adopted to eliminate sudden spikes in measured distances [6]. The filter is defined as follows:

$$y[n] = \frac{1}{N} \sum_{K=0}^{N-1} X[n-K] \tag{4}$$

$y[n]$ is the filtered output at sample n, $X[n-K]$ is the K-th raw data point within the window, N is the window size (number of data points).

4.2. Following control strategy

In this design, the cart's following control strategy uses real-time UWB positioning data to adjust its motion so that it maintains a preset distance from the target and dynamically tracks the target as it moves. The control framework adopts proportional control (P-control) combined with segmented differential steering, achieving low-complexity yet highly reliable motion control. The logical structure is described below.

4.2.1. Proportional control

Proportional (P) control is a linear control method in which the controller output is directly proportional to the instantaneous error. It features fast response, simple structure, and easy implementation. If necessary, integral (I) and derivative (D) terms can be added to improve dynamic performance, but proportional control alone is suitable for this simplified following task.

The implementation steps in this design are as follows:

(1) Error computation

$$error = d_{target} - d_{current} \tag{5}$$

where d_{target} is the preset following distance and $d_{current}$ is the measured distance.

(2) PWM signal generation

$$PWM = K_p \times error \tag{6}$$

where K_p is the proportional gain determined experimentally. The PWM output must be limited to a safe range to prevent motor overload.

4.2.2. PWM-based motor speed control

Pulse Width Modulation (PWM) is an efficient technique that uses digital signals to achieve precise analog-equivalent control. When regulation of voltage or current is required, PWM adjusts the duty cycle of a periodic pulse signal to generate the desired control effect. As a key technique in microcontroller systems, PWM converts discrete digital pulses into continuous-equivalent actuation for inertial loads such as motors.

PWM signals are characterized by three core parameters: Frequency, which determines the signal period, Duty cycle, which represents the proportion of time the signal remains high, and Period, the inverse of frequency. Together, these parameters define the waveform of the control signal.

In this design, the motor speed is controlled by dynamically adjusting the PWM duty cycle. With the drive voltage amplitude held constant, varying the duty cycle effectively changes the average voltage applied to the armature, enabling fine-grained control of motor speed.

By adjusting the duty cycle of the signal, you can control the motor speed or LED brightness. The duty cycle *D* is calculated as follows:

$$D = \frac{CCR}{ARR=1} \times 100\% \tag{7}$$

where the Capture/Compare Register (CCR) sets the duty cycle of the PWM signal, allowing flexible control of the motor's energization duration. The Auto-Reload Register (ARR) defines the PWM period. The two registers work together to provide precise waveform control and ensure smooth motor operation [6].

A higher duty cycle increases the motor's average voltage and thus its speed; reducing the duty cycle slows the motor down. In this design, the PWM output is constrained within the range of 20%–80% to prevent excessive motor load.

5. Experimental testing

5.1. Positioning experiment

In the positioning accuracy experiment, the distance between the two base stations was set to be identical to the installation spacing on the cart. The UWB tag was manually moved to simulate the cart's positional changes. Base Station 0 was connected to a computer through a serial port, allowing the upper-computer software to display real-time measurement data, as shown in Figure 7.

To ensure reliable testing conditions, the line-of-sight between the tag and the base stations was kept unobstructed throughout the experiment to avoid signal blockage. The installation heights of the tag and the base stations were also maintained at the same level to eliminate the influence of height variation on positioning results. The experiment setup is shown in Figure 8.

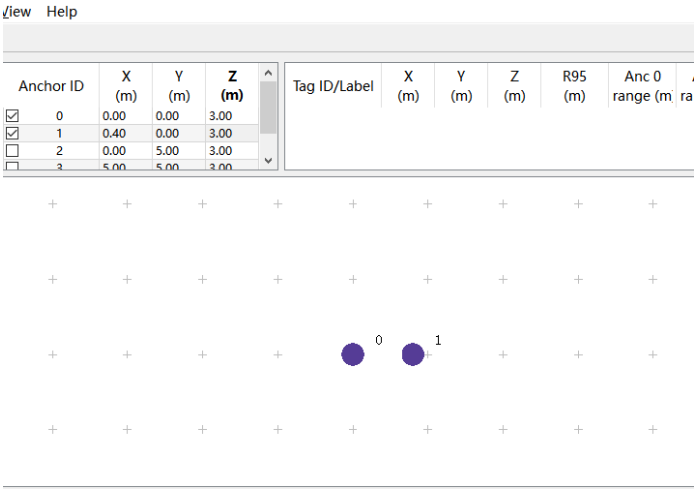

Figure 7. Upper-computer software interface

Figure 8. Positioning experiment setup

For each measurement point, 10 repeated measurements were conducted to minimize random errors. The arithmetic mean of the 10 measurements was taken as the representative value for each point. Data from nine test points were then imported into plotting software to generate a polar plot, providing a visual representation of the positioning performance at all test locations (Figure 9).

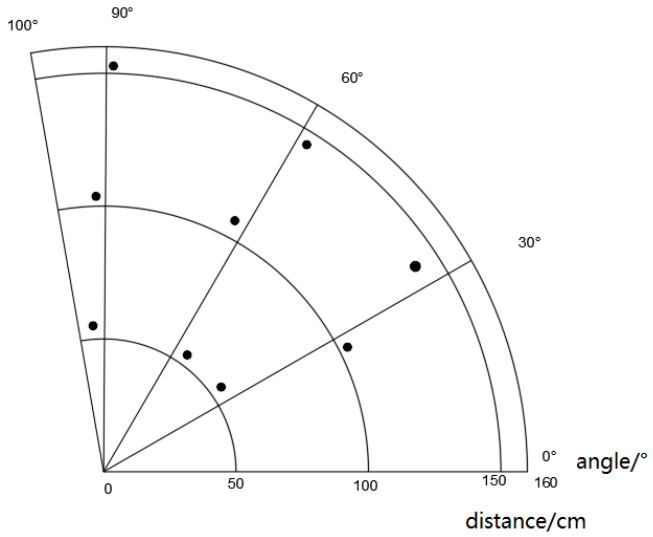

Figure 9. Positioning test results (polar plot)

The positioning error at each test point was calculated based on the deviation between the theoretical and measured distances. The results show that the maximum average distance error was less than 9 cm, meeting the design requirement for ranging accuracy.

For angle estimation, the maximum average angular error was less than 10°, which also satisfies the expected directional measurement performance. Overall, the experimental results demonstrate that the positioning system delivers reliable distance and angle estimation capabilities suitable for indoor tracking applications.

5.2. Following experiment

The main objective of the following experiment was to verify the stability and reliability of the cart's real-time dynamic following function. The experiment was conducted at the junction of a dormitory corridor and stairwell, an area with moderate path complexity (Figure 10). During the test, a participant held the UWB tag and walked along a predefined path at an approximately constant speed of 0.3 m/s, while the cart autonomously followed based on the tag's position [7, 8].

To maintain safe operation, a minimum safety distance between the cart and the tag was always maintained. The movement trajectories of both the participant and the cart were recorded, and the cart's actual motion path was plotted after the experiment (Figure 11), providing an intuitive view of its dynamic following behavior.

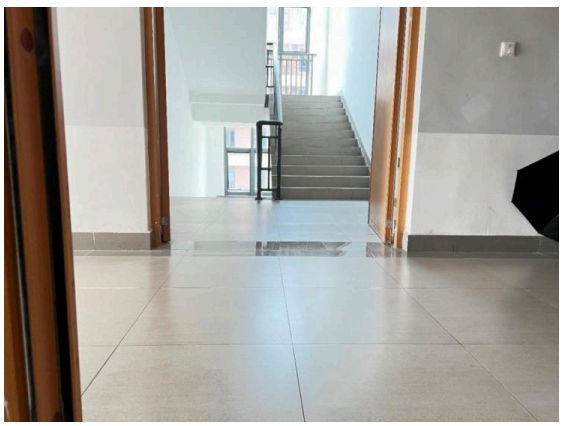

Figure 10. Experimental environment

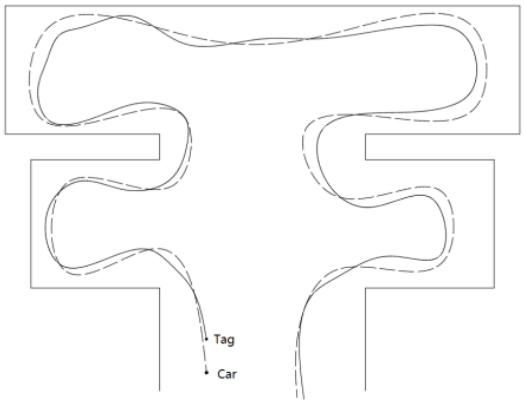

Figure 11. Cart trajectory

The completed experiment confirms that the cart successfully achieves autonomous following. As shown in the trajectory plot, overall tracking performance is stable. However, slight response delays and fluctuations were observed during turning motions. The reasons are primarily as follows:

(1) Since the tag was carried by a human, unavoidable hand and body movements introduced jitter in distance measurements.

(2) The positioning algorithm assumes that the tag and base stations lie on the same horizontal plane. In the actual test, this condition was not strictly met, resulting in measured distances being slightly smaller than the true values.

6. Conclusion

This design targets practical following requirements in modern logistics scenarios, integrating UWB high-precision positioning technology with relevant ranging algorithms and an STM32-based embedded control system to develop an autonomous following transport cart. The complete system—including structural assembly, hardware circuit design, and control program development—was successfully implemented. Through carefully designed experiments, the system's positioning accuracy and following stability were verified, and stable autonomous following was ultimately achieved. However, the current positioning model is a simplified one-dimensional scheme. Future work may include deploying additional base stations and incorporating trilateration to achieve two-dimensional coordinate estimation, while optimizing base station layout to reduce system cost. For high-speed dynamic targets, additional improvements are needed to address latency caused by UWB data update rate and control cycle limitations.

References

[1] Chen, K. (2023). *Research on localization and navigation of a picking robot based on multi-sensor fusion* [Master's thesis, Chengdu University of Technology].

[2] Xu, S. (2022). *Design of an intelligent vehicle formation system based on UWB* [Master's thesis, Nanjing University of Information Science and Technology].

[3] Qu, J. (2023). A review of UWB indoor positioning. *Journal of Physics: Conference Series, 2669*(1), Article 012034. https: //iopscience.iop.org/article/10.1088/1742-6596/2669/1/012034

[4] Gu, Y. (2018). *Research and design of an indoor robot positioning system based on UWB* [Master's thesis, Harbin Institute of Technology].

[5] Wei, Y.-F., Xuan, Y.-T., & Meng, R. (2024). Design of a tracked automatic-following vehicle. *Intelligent Computer and Applications, 14*(6), 193–196.

[6] Liu, L., Xie, J., Wu, W., Chen, S., & Li, H. (2021). Design of an intelligent logistics car based on STM32. *Journal of Physics: Conference Series, 1952*(4), Article 042040. https: //iopscience.iop.org/article/10.1088/1742-6596/1952/4/042040

[7] Zhang, C. (2022). *Design and research of a heavy-load AGV positioning system based on UWB* [Master's thesis, Taiyuan University of Science and Technology].

[8] Zhao, R., Zhang, H., & Qi, F. (2024). Intelligent following car based on ultra-wideband technology. *Journal of Physics: Conference Series, 2816*(1), Article 012053. https: //iopscience.iop.org/article/10.1088/1742-6596/2816/1/012053